Neuron, Vol. 48, 315–327, October 20, 2005, Copyright ©2005 by Elsevier Inc. DOI 10.1016/j.neuron.2005.09.022

Somatosensory Integration Controlled by Dynamic Thalamocortical Feed-Forward Inhibition

Laetitia Gabernet,[1] Shantanu P. Jadhav,[2] Daniel E. Feldman,[2] Matteo Carandini,[3] and Massimo Scanziani[1,2,*]
[1]Brain Research Institute
University of Zurich
8057 Zurich
Switzerland
[2]Neurobiology Section
Division of Biology
University of California, San Diego
La Jolla, California 92093
[3]Smith-Kettlewell Eye Research Institute
San Francisco, California 94115

Summary

The temporal features of tactile stimuli are faithfully represented by the activity of neurons in the somatosensory cortex. However, the cellular mechanisms that enable cortical neurons to report accurate temporal information are not known. Here, we show that in the rodent barrel cortex, the temporal window for integration of thalamic inputs is under the control of thalamocortical feed-forward inhibition and can vary from 1 to 10 ms. A single thalamic fiber can trigger feed-forward inhibition and contacts both excitatory and inhibitory cortical neurons. The dynamics of feed-forward inhibition exceed those of each individual synapse in the circuit and are captured by a simple disynaptic model of the thalamocortical projection. The variations in the integration window produce changes in the temporal precision of cortical responses to whisker stimulation. Hence, feed-forward inhibitory circuits, classically known to sharpen spatial contrast of tactile inputs, also increase the temporal resolution in the somatosensory cortex.

Introduction

Timing is a basic attribute of sensory stimuli and needs to be faithfully represented by the nervous system to allow accurate stimulus identification and discrimination. Accordingly, temporal features of stimuli are accurately encoded and conveyed through the thalamus to the sensory cortex in several different sensory modalities (Arabzadeh et al., 2005; Buracas et al., 1998; DeWeese et al., 2003; Phillips et al., 1988; Reinagel and Reid, 2000; Wehr and Zador, 2003). For example, the timing of spikes in somatosensory cortex precisely reflects the temporal sequence of stimuli generated while touching an object (Phillips et al., 1988), and moment-to-moment changes in spiking probability of barrel cortex neurons precisely reflect instantaneous variations in the velocity of a whisker sweeping over a surface (Arabzadeh et al., 2005).

Although this temporal precision is likely to be crucial for sensory representation, the cellular mechanisms that enable cortical neurons to follow the temporal structure of their thalamic inputs with such fidelity is currently unknown. In the cortex, individual thalamic afferent fibers impinging on principal neurons mediate excitatory postsynaptic potentials (EPSPs) that are small (Gil et al., 1999; Stratford et al., 1996) compared to the depolarization necessary to trigger a spike (Brecht and Sakmann, 2002). Hence, EPSPs resulting from several fibers have to summate to reach threshold for action potential generation. The time window within which EPSPs can effectively summate (Lloyd, 1946) is called the integration window (IW). The shorter the IW, the more coincident the activity of presynaptic fibers has to be to trigger a spike (Koch et al., 1996; Konig et al., 1996; Pouille and Scanziani, 2001). The IW, thus, dictates how precisely the activity of a neuron can report the temporal structure of the activity of its inputs.

To establish the basis for spike timing precision in the initial steps of sensory processing in the somatosensory cortex, we determined the cellular mechanisms that control the IW of principal (excitatory) layer 4 neurons to thalamic inputs. Here, we demonstrate that the IW of layer 4 principal neurons has a broad dynamic range that can vary over an order of magnitude in an activity-dependent manner. The duration of the IW is dynamically regulated by an efficient and temporally precise thalamocortical feed-forward inhibitory circuit. Feed-forward inhibitory circuits are well known to participate in the enhancement of spatial contrasts of somatosensory stimuli (Mountcastle, 1968; Mountcastle and Powell, 1959). Our data show that these circuits also enforce and modulate temporal resolution of tactile information.

Results

Dynamic Control of Spike-Timing Precision in Barrel Cortex In Vivo

Spiking responses of regular spiking (RS) units, which represent presumed excitatory neurons in layer 4 of barrel cortex, were measured for low frequency (0.5 Hz) principal whisker (PW) deflections in anesthetized rats. Spikes were tightly time locked to the stimulus (jitter, 4.05 ± 0.28 ms; n = 105) (Figure 1A), despite occurring with relatively low probability (0.25 ± 0.02), consistent with previous observations of high temporal precision in barrel cortex (Arabzadeh et al., 2005; Petersen et al., 2001; Shimegi et al., 1999). Repetitive stimulation of the whisker at 10 Hz, similar to natural whisking frequency, however, led to a significant increase in jitter of layer 4 RS units (jitter; fourth stimulus, 5.79 ± 0.32 ms [$p < 0.01$]; sixth stimulus, 7.93 ± 0.43 ms [$p < 0.001$]; paired t test; n = 105) (Figures 1B and 1C), along with an adaptation (decrease in spike probability) and increased latency. To determine whether the increase in spike jitter reflects dynamic changes in the thalamocortical circuit, rather than in the periphery or the brainstem, we recorded from thalamic units in the VPM nucleus, which provide input to layer 4. VPM units showed virtually no increase in jitter during 10 Hz principal whisker stimulation, indicating that the temporal precision of

*Correspondence: massimo@ucsd.edu

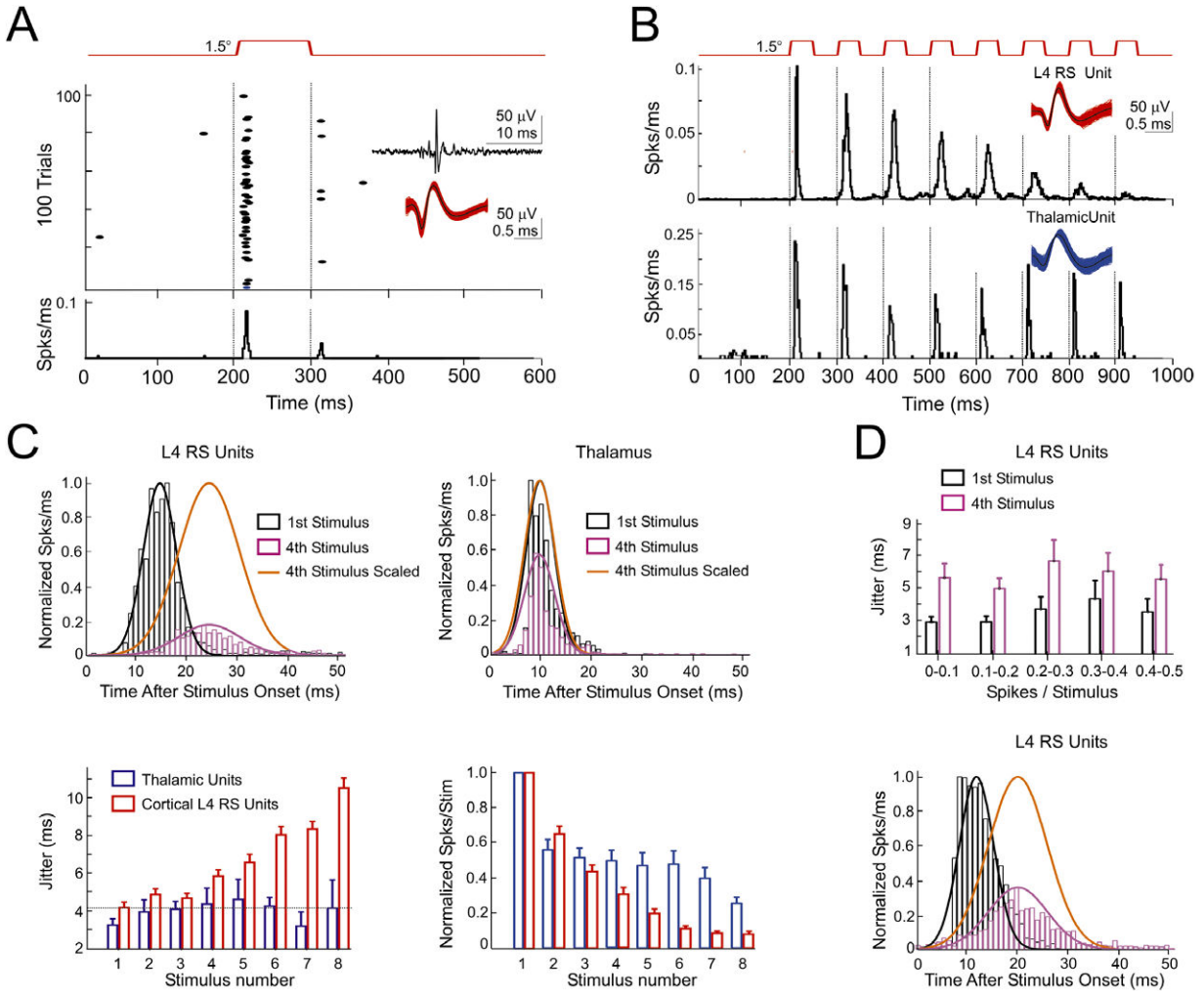

Figure 1. Increased Spike Jitter of Layer 4 RS Units In Vivo by Repetitive Whisker Stimulation

(A) Raster plot and peri-stimulus time histogram (PSTH) of the response of a single RS unit to PW deflection (1.5°, 0.5 Hz, 100 trials). Insets: raw voltage recording and representative spike waveforms (red) and mean waveform (black) for the RS unit after spike sorting.

(B) PSTHs of the responses of a layer 4 RS unit and a thalamic (VPM) unit to 10 Hz principal whisker (PW) deflection. Note the pronounced adaptation (decrease in spike probability) and increase in jitter (width of the PSTH peaks) of the RS unit as compared to the thalamic unit. Insets: single-unit spike waveforms.

(C) Effects of 10 Hz stimulation across the population of layer 4 RS and thalamic units. Top: population PSTHs for onset responses to first and fourth stimuli in the 10 Hz train. Curves represent Gaussian fits. Note the increased jitter in layer 4 RS cells, but not in thalamus. Bottom left: spike jitter increased with stimulus number in the train for RS units (increase in jitter was significant after the fourth stimulus in the train, $p < 0.01$, paired t test), but not for thalamic units. Bottom right: adaptation of whisker-evoked spike count (normalized to first stimulus in each unit) for the population of RS (n = 105) and thalamic units (n = 22). RS units adapted significantly faster than thalamic units (RS, adaptation index [AI; defined as the ratio of fifth stimulus response to first stimulus response] = 0.19 ± 0.03; thalamus, AI = 0.47 ± 0.07; $p < 0.001$, t test).

(D) Increase in jitter during trains is not due to decreased spike count. Top: jitter for RS units grouped by whisker-evoked spike count to the first stimulus. Increase in jitter occurred equally for the strongest responding and the weakest responding units. Bottom: population PSTHs for first and fourth stimuli for RS units tested with a longer recovery time between each train (10 s, n = 22) to produce less adaptation. Note the marked increase in jitter despite less adaptation. Summary graphs show mean ± standard error of the mean (SEM).

cortical spiking responses is dynamically regulated downstream of the thalamus. Because 10 Hz whisker stimulation reduced whisker-evoked spikes for RS units (Chung et al., 2002; Khatri et al., 2004) (Figures 1B and 1C), the increased jitter could merely reflect weaker excitatory input to RS units or increased contamination of weak whisker-evoked responses by spontaneous spikes. To address this possibility, we tested whether spike jitter was correlated with spike probability across RS units. No correlation existed (r = 0.04) (Figure 1D). In addition, an identical increase in jitter occurred when long recovery times were used between 10 Hz trains, a protocol that leads to less adaptation and more spikes (Figure 1D). Thus, the increase in spike jitter during trains was not due to reduced excitation of RS neurons or the small number of whisker-evoked spikes.

These data show that the temporal precision of cortical responses to somatosensory stimuli is dynamically regulated by a circuit downstream of the thalamus. To establish what controls this dynamic range, we determined the integration window (IW) of cortical units to thalamic inputs in vitro.

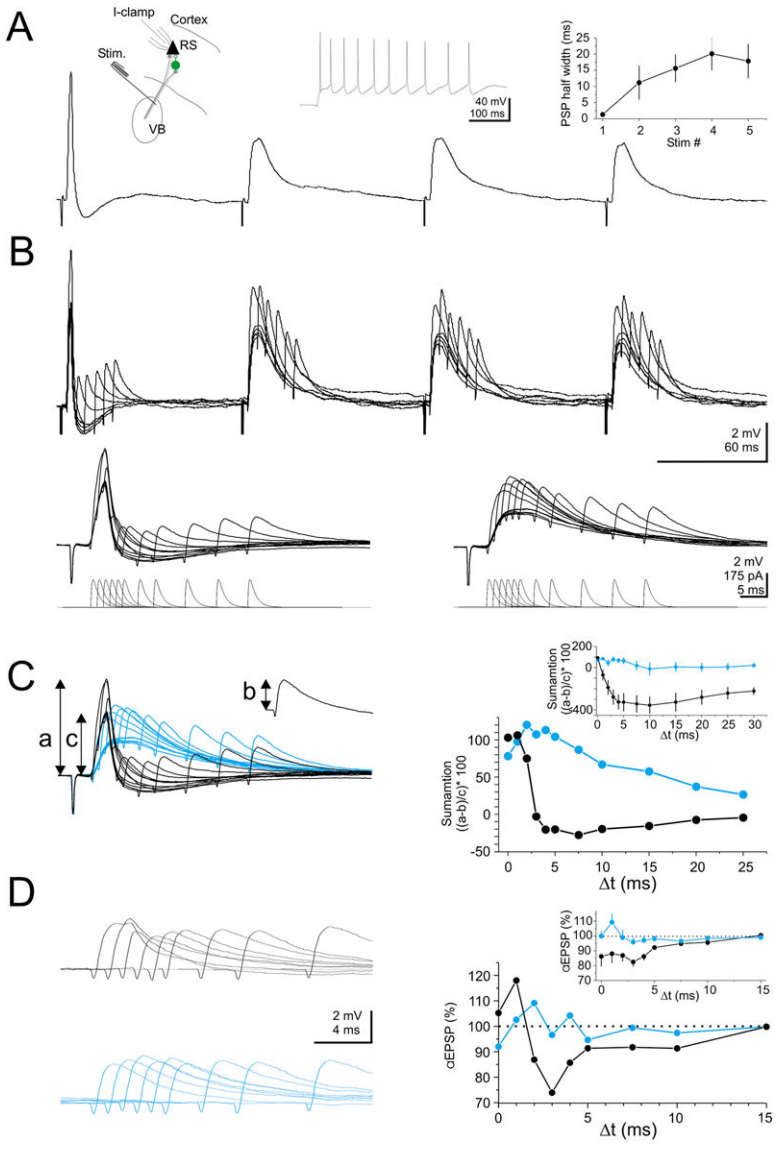

Figure 2. Shift in the Integration Window of Layer 4 Regular Spiking Neurons

(A) Voltage response of a layer 4 RS neuron to four stimuli delivered at 10 Hz to the thalamus (Vm = 70 mV). Insets. Left, schematic of the recording configuration (RS neuron, black; inhibitory neuron, green; VB, ventrobasal complex). Center, spiking pattern of the neuron in response to a positive square pulse of current (+550 pA). In the following figures, the spiking pattern allowing identification of the neurons as RS or FS is shown as an inset. Right, the half width of the postsynaptic potential is plotted against stimulus number (n = 7–8);

(B) Top, six superimposed sweeps with artificial EPSPs (aEPSPs) triggered at different intervals after thalamic stimulation. Bottom, enhanced time scale for the first (left) and last stimulus. Eleven superimposed sweeps are shown together with the time course of current injection (lower traces).

(C) Left, the response of the neuron to the first (black) and last (blue) thalamic stimuli (same as in [B]) are superimposed to illustrate the different integration window. Right, the summation of the thalamic and aEPSPs for the first (black) and last (blue) stimuli is computed as the peak of the summed response (a) minus the peak of the aEPSP evoked alone (b) and normalized by the peak of the thalamic response (c). The result is plotted against the interval (Δt) between the onset of the thalamic and artificial EPSPs. Inset, summary graph (n = 6).

(D) Left, aEPSPs evoked at different intervals after thalamic stimulation were "isolated" by subtracting the thalamic response. First stimulus, black traces; last stimulus, blue traces. Note the reduction of the aEPSP amplitude for short intervals after the first stimulus. Right, the amplitude of the aEPSP is plotted against the interval (Δt) between the onset of the thalamic and artificial EPSPs for the first (black) and last (blue) stimuli. Inset, summary graph (n = 6). Summary graphs show mean ± SEM.

Dynamic Integration Window in Cortical RS Neurons

To determine the IW of cortical neurons to thalamic inputs, we recorded from layer 4 RS neurons in thalamocortical slices and stimulated their thalamic afferents with an extracellular electrode placed in the ventrobasal complex (VB; see Experimental Procedures). Thalamic stimulation evoked an EPSP/IPSP sequence, consistent with previous reports (Agmon and Connors, 1991; Gil and Amitai, 1996; Porter et al., 2001). Artificial excitatory postsynaptic potentials (aEPSPs) were evoked in RS neurons (with either current or dynamic clamp; see Experimental Procedures) at different intervals after thalamic stimulation.

RS neurons exhibited a very narrow IW to thalamic inputs. To effectively summate (i.e., to depolarize the membrane more than the peak-positive value of the thalamic response), we had to evoke aEPSPs within ~1 ms (range, <1 to 3 ms; n = 6) after the onset of the thalamic EPSP (Figures 2A–2C). An IW of 1 ms is extremely narrow, particularly when compared with the membrane time constant (17 ± 1 ms; n = 9). This result suggests that RS neurons operate as coincidence detectors.

The IW, however, was broadened by a factor of ten after repetitive stimulation. Repetitive thalamic stimulation at 10 Hz led to a pronounced and reversible increase in the IW by about one order of magnitude (to ~10 ms after four to five stimuli; range 3 to >25 ms; n = 6) (Figure 2C). This broadening of the IW was caused by an increase in the half width of thalamically evoked postsynaptic potentials (PSPs; from 1 ± 0.3 ms after the first stimulus to 20 ± 5 and 18 ± 5 ms after the fourth and fifth, respectively; n = 8) (Figure 2D) and by a reduction in the shunt (Coombs et al., 1955) of aEPSPs evoked shortly after the onset of thalamic EPSPs (first stimulus, 17% ± 3% reduction of aEPSP amplitude; fifth stimulus, 4% ± 3% reduction) (Figure 2). Both effects—the increase in half width of the thalamic PSP and the decrease in the shunt—could be explained if repetitive stimulation reduced synaptic inhibition.

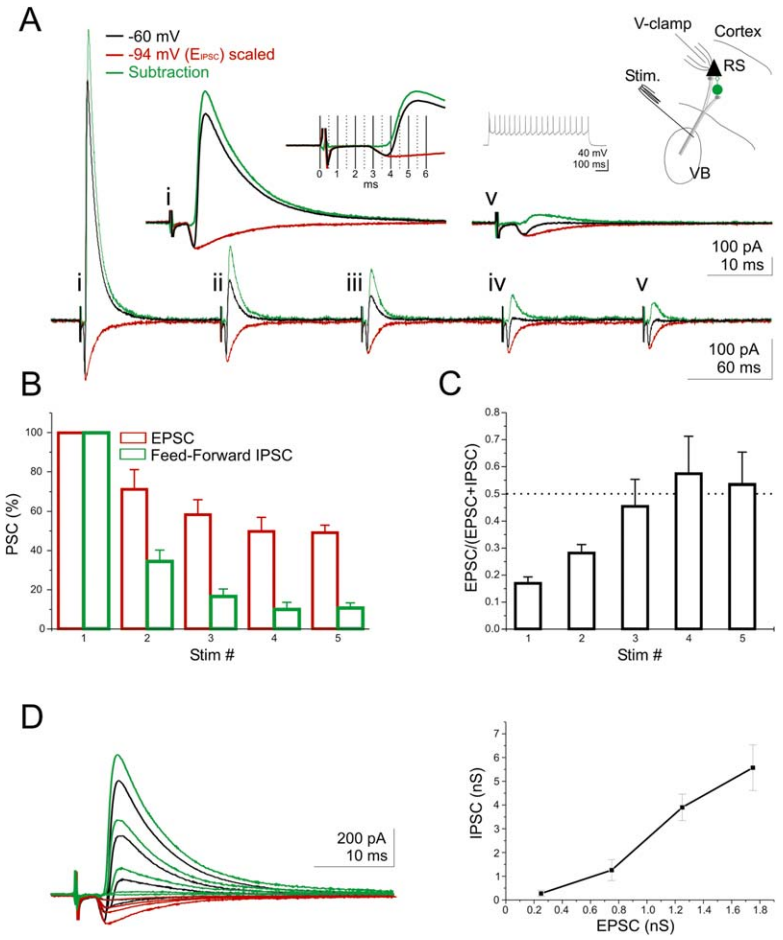

Figure 3. Broad Dynamic Range of Thalamocortical Feed-Forward Inhibition

(A) Response to 10 Hz thalamic stimulation of a layer 4 RS neuron voltage clamped at –60 mV (black trace) and at the IPSC reversal potential (red trace; the first EPSC on the red trace is scaled to the first EPSC on the black trace). The feed-forward IPSC (green trace) was isolated by subtracting the red trace from the black trace. The inset shows the responses to the first and last thalamic stimuli on an expanded time scale. Note the ~1ms delay between the onset of the thalamic EPSC and the onset of the feed-forward IPSC.

(B) Summary graph of the EPSC and IPSC amplitude plotted against stimulus number (n = 8 for IPSC and 7 for EPSC). Note that although the thalamic EPSC decreases to ~50% of its initial amplitude, feed-forward inhibition is reduced by ~90%.

(C) Change in the excitation-inhibition ratio (peak conductances) plotted against stimulus number (n = 7).

(D) EPSC-IPSC sequences recorded at five different stimulation intensities (left, same cell as above) and summary graphs (right) in which the peak conductance of the IPSC is plotted against the conductance of the EPSC (n = 5–6; bins, 0–0.249 nS; 0.25–0.749 nS; 0.75–1.249 nS; 1.25–1.75 nS). Note that disynaptic feed-forward IPSCs can be elicited even when direct thalamic EPSCs are very small. Summary graphs show mean ± SEM.

We asked whether repetitive stimulation of VB would affect the amplitude of thalamocortical feed-forward inhibition. RS neurons were voltage clamped at −60 mV, i.e., between the reversal potentials for excitatory and inhibitory postsynaptic currents. VB stimulation elicited an EPSC followed with a delay of 1.2 ± 0.1 ms (n = 11) by an IPSC (Figure 3A). The brief delay between EPSC and IPSC indicates that IPSCs were triggered in a feed-forward, disynaptic manner, i.e., by thalamic excitation of cortical GABAergic interneurons rather than by a feedback recruitment of interneurons via cortical RS neurons. The EPSC-IPSC sequence could be elicited even at very low stimulation intensities and the ratio between the peak EPSC and IPSC conductances was stable over a relatively wide range of stimulation intensities (Figure 3D). Repetitive 10 Hz thalamic stimulation, however, altered this balance through a striking decrease in the amplitude of feed-forward IPSCs. Although after five stimuli, EPSC amplitude decreased by 51% ± 4% (n = 7), feed-forward IPSCs decreased by 89% ± 3% (n = 8) (Figures 3A and 3B). Repetitive stimulation, therefore, increased the ratio between excitation and inhibition in RS neurons. Repetitive stimulation, moreover, progressively increased the delay between the EPSC and IPSC to 2.1 ± 0.4 ms (n = 5) after the fifth stimulus.

These data show that in the barrel cortex, thalamocortical feed-forward inhibition operates over a very broad dynamic range, allowing RS neurons to shift from coincidence detection to integration. We next determined the cellular basis of this dynamic range.

Mechanism Underlying the Dynamics of Thalamocortical Feed-Forward Inhibition

The activity-dependent reduction in the amplitude of thalamocortical feed-forward inhibition and the resulting increase in IW could be due to the depression of two distinct synapses: the glutamatergic synapse from thalamus to interneurons, or the GABAergic synapse from interneurons onto RS neurons. Depression of the second synapse would directly affect the amplitude of feed-forward inhibition; depression of the first synapse would reduce the fraction of interneurons that are excited above threshold for action potential generation and thus participate in the generation of feed-forward inhibition.

We addressed both possible mechanisms by directly recording from GABAergic interneurons. Because layer 4 inhibitory fast spiking (FS) neurons are directly excited by thalamic inputs (Gibson et al., 1999; Keller and White, 1987; Staiger et al., 1996) and inhibit RS neurons (Beierlein et al., 2003; Tarczy-Hornoch et al., 1998), they are likely to represent the predominant source of thalamocortical feed-forward inhibition. We thus recorded from connected FS to RS neurons pairs.

FS neurons showed functional connections with approximately 50% of neighboring RS neurons. Unitary

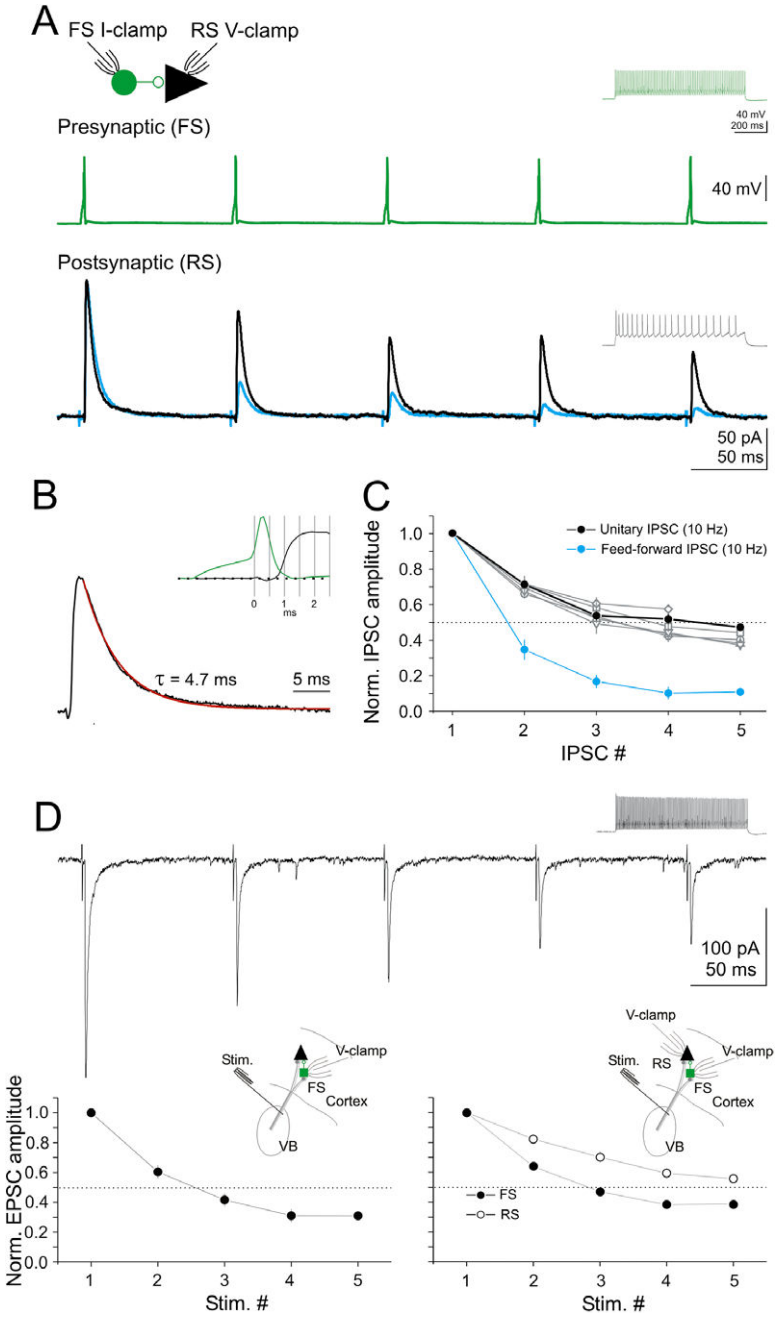

Figure 4. Dynamics of the Input and the Output of Cortical FS Neurons

(A) Paired recording between a presynaptic FS (green) and a postsynaptic RS (black) neuron. Brief current pulses were injected in the FS neurons to trigger series of five action potentials at 10 Hz. Note that the resulting unitary IPSCs in the RS neuron depress to a much lesser extent than feed-forward IPSCs evoked with thalamic stimulation (superimposed blue trace, same as in Figure 3A).

(B) Unitary IPSC from (A) on an expanded time scale. A monoexponential fit (red trace) is superimposed on the decay phase. The inset illustrates the delay between the presynaptic spike and the postsynaptic response.

(C) Summary graph of unitary IPSC amplitude plotted against presynaptic spike number. Black solid circles, unitary IPSCs evoked at 10 Hz (n = 6); open symbols, unitary IPSCs evoked at 5 Hz (diamonds; n = 5), 20 Hz (down triangles; n = 5), 50 Hz (up triangles; n = 5), 100 Hz (squares; n = 5), 200 Hz (circles; n = 2). The reduction in amplitude of feed-forward IPSCs (blue solid circles; from Figure 3B) evoked with thalamic stimulation at 10 Hz is included, for comparison.

(D) Current trace, EPSCs recorded in an FS neuron ($V_{holding}$, −60 mV) in response to five thalamic stimuli delivered at 10 Hz. Summary graphs. Left, thalamic EPSC amplitude for nine similar experiments plotted against stimulus number. Right, thalamic EPSC amplitude recorded simultaneously in FS (solid symbols) and RS (open symbols) neurons plotted against stimulus number (n = 5). Summary graphs show mean ± SEM.

IPSCs triggered by individual FS neuron spikes occurred without failures, had an average peak conductance of 2.8 ± 0.85 nS (n = 6), and decayed with a time course of 6.2 ± 2.5 ms (Figure 4A). The decay of the unitary IPSCs was not significantly different than the decay of feed-forward inhibition (6.5 ± 0.62 ms; n = 10; p = 0.79) evoked by thalamic stimulation, consistent with the idea that layer 4 FS neurons are the predominant mediator of thalamocortical feed-forward IPSCs. The latency between the action potential (steepest point in its rising phase) triggered in the FS neurons and the onset of unitary IPSCs (5% of peak amplitude) recorded in the RS neuron averaged 0.6 ± 0.03 ms (n = 5). This indicates that the first half of the 1.2 ms delay between the EPSP and the feed-forward IPSC determined above is used for thalamic EPSPs to reach threshold for action potential generation in FS neurons, whereas the second half is taken by spike propagation and GABA release.

Depression at the synapse from FS to RS neurons was pronounced but not enough to account for the reduction in thalamocortical feed-forward inhibition with repetitive thalamic stimulation. Trains of spikes triggered at 10 Hz in FS cells resulted in unitary IPSCs that depressed to 47% ± 1% of their original amplitude after the fifth stimulus (Figures 4A and 4C). Even when triggered at higher frequencies, unitary IPSCs did not depress to less than ~40% (Figure 4C). The dynamics of the GABAergic synapses, therefore, cannot account for the observed ~90% reduction in thalamocortical feed-forward inhibition.

These results suggest that during repetitive thalamic stimulation, progressively fewer FS neurons participate in mediating feed-forward inhibition after each stimulus in the train. By comparing the depression of unitary IPSCs (uI_5/uI_1) with the decrease in thalamically evoked feed-forward inhibition (FFI_5/FFI_1), one can estimate the maximal fraction of GABAergic interneurons still participating in feed-forward inhibition by the fifth stimulus (N_5/N_1) to be only about 20% of those active at the beginning of the train ($FFI_5/FFI_1 = [uI_5/uI_1] \times [N_5/N_1]$).

We thus tested the possibility that excitation of FS neurons by thalamic afferents may depress during repetitive thalamic stimulation, thereby reducing the fraction of recruited interneurons. When elicited at 10 Hz, thalamic EPSCs recorded in FS neurons showed a marked depression (to 31% ± 3% of the original amplitude after five stimuli; n = 9) (Figure 4D) that was, in fact, significantly larger than the depression of thalamic EPSCs onto RS neurons (to 49% ± 4%; n = 7; see Figure 3; p = 0.0014). We confirmed this target cell specificity in thalamic EPSC depression by recording thalamic EPSCs simultaneously in FS and RS neurons. Again, thalamic EPSCs recorded in FS neurons depressed significantly more than those recorded in RS neurons (to 39% ± 2% versus 56% ± 3%; n = 5; p = 0.013) (Figure 4D).

These results indicate that the broad dynamic range of thalamocortical feed-forward inhibition is primarily achieved by varying the fraction of thalamically recruited FS neurons and, to a lesser extent, by the dynamics of the FS to RS synapse.

Thalamic Excitation of Cortical GABAergic Interneurons

For feed-forward inhibition to effectively control the IW of RS neurons, it is expected that action potentials are readily triggered in FS neurons also in response to relatively weak thalamic stimuli.

Figure 3D shows that this is indeed the case as feed-forward inhibition on RS neurons can be triggered even at low stimulation intensities, when the average peak conductance of thalamic EPSCs recorded in RS neurons is below 0.25 nS. This suggests that either activation of a limited number of thalamic fibers is sufficient to trigger a spike in FS neurons or FS neurons have a higher probability of being contacted by a thalamic fiber than RS neurons. We addressed both possibilities.

If the probabilities of a thalamic axon to form synaptic contacts with FS and RS neurons are similar, the ratio of the amplitude of unitary thalamic EPSCs (EPSCs evoked by stimulating a single thalamic fiber [Beierlein and Connors, 2002]) recorded in FS and RS neurons should be similar to the ratio of the amplitude of compound EPSCs (EPSCs evoked by stimulating several thalamic fibers). Minimal stimulation of the thalamus was used to isolate unitary thalamic EPSCs in FS and RS neurons. The amplitude of unitary thalamic EPSCs was defined as the amplitude of the successes measured over a stimulation range in which, starting from failures only, increasing stimulation intensity reduced failure rate without affecting the average amplitude of successes. Unitary thalamic EPSCs recorded in FS neurons had a peak amplitude that was 3.5 times larger than the one recorded in RS neurons (FS neurons, 200 ± 42 pA; n = 6; RS neurons, 57 ± 15 pA; p = 0.023; n = 4) (Figures 5A and 5B). EPSC recorded in FS neurons also had faster decay kinetics than EPSC in RS neurons (1.5 ± 0.3 ms versus 4.5 ± 0.4 ms; $p = 3.35 \times 10^{-5}$) consistent with the different kinetics of AMPA receptors expressed in these neurons (Jonas et al., 1994). Strikingly, also the amplitude of compound EPSCs recorded simultaneously in FS and RS neurons was 3.5 ± 0.6 times larger in FS neurons (n = 6), indicating that thalamic fibers contact FS and RS neurons with similar probabilities (Figures 5C and 5D).

The experiment shown in Figure 5A also demonstrates that an individual thalamic afferent can contact both FS and RS neurons. In this particular example, not only were the minimal stimulation criteria satisfied for both neurons simultaneously, but failures and successes were absolutely correlated, indicating that they were contacted by the same fiber.

We then determined the minimal number of thalamic fibers necessary to trigger a spike in FS neurons. For this, we compared the amplitude distribution of unitary EPSCs with the average size of thalamic EPSCs on FS neurons when stimulating the thalamus at threshold to induce feed-forward inhibition in simultaneously recorded RS neurons. Clearly, the distribution of the amplitudes of unitary EPSCs (range, 51–289 pA) (Figure 6) was similar to the distribution of the amplitudes of EPSC (average, 170 ± 64 pA; range 52–400 pA; n= 5) (Figure 6) recorded in FS neurons when stimulating at threshold for eliciting feed-forward inhibition in RS neurons. A comparison between the lower and the higher values in the two distributions of EPSC amplitudes suggests that one to eight thalamic fibers are sufficient to trigger a spike in FS neurons. Thus, even a single thalamic fiber can evoke feed-forward inhibition.

These data show that despite the similar probabilities of thalamic neurons to contact FS and RS neurons, strong thalamic input on FS neuron ensures efficient feed-forward inhibition and an accordingly narrow IW even in response to very weak thalamic activity.

Temporal Precision of FS Neurons

Despite the reduced fraction and increased delay of FS neuron recruitment, FS neuron activity remained remarkably synchronous during repetitive thalamic stimulation (Figures 7A and 7B). To estimate the degree of synchrony of FS neurons recruited after each thalamic stimulus, we deconvolved the time course of feed-forward inhibition recorded in RS neurons with the time course of a "standard" unitary IPSC (i.e., the averaged time course of unitary IPSCs recorded in our six connected FS to RS pairs) (Figure 7A). This analysis indicates that 50% of FS neurons spiked within a window of 0.22 ± 0.23 ms during the first response and within a window of 0.52 ± 0.41 ms during the fifth response of a train (n = 8). These results show that the degree of synchrony of FS neurons is only slightly affected by ongoing thalamic activity.

Spiking of FS Neurons In Vivo

The dynamic properties of the thalamocortical feed-forward inhibitory circuit observed in vitro leads to two predictions in the intact animal. First, because of the strong depression of the thalamus to FS synapse, repetitive whisker stimulation will markedly reduce spike

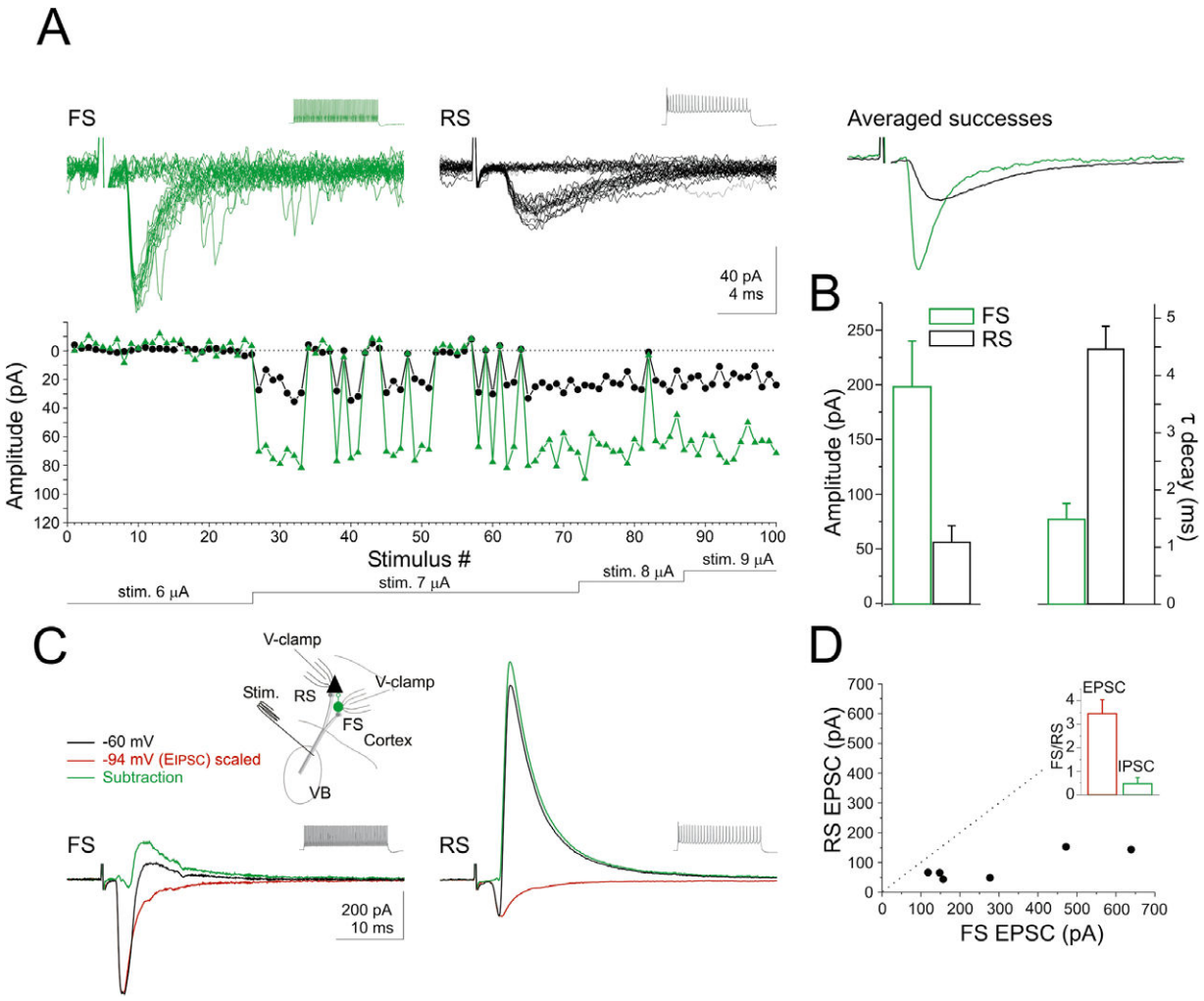

Figure 5. Functional Divergence of Thalamic Afferents onto FS and RS Neurons

(A) Simultaneous voltage clamp recording ($V_{holding}$, −77 mV) from an FS (green traces) and RS (black traces) neuron during minimal stimulation of the thalamus (23 superimposed individual sweeps each). Stimuli were delivered at 0.2 Hz. The amplitude of the EPSC is plotted against stimulus number. The intensity of stimulation is plotted below the graph. Note that increasing stimulation intensity reduces failures without affecting the amplitude of successes. Also note that failures and successes in FS and RS neurons are concurrent.

(B) The amplitude and decay kinetics of minimally evoked EPSCs recorded in FS (green; n = 6) and RS (black; n = 4) neurons. With the exception of the experiment illustrated in (A), for the rest of the experiments, minimal stimulation conditions were satisfied for only one neuron at the time.

(C) Simultaneous recording from a FS and RS neuron in response to "nonminimal" thalamic stimulation. Both neurons were voltage clamped at −60 mV (black trace) and at the IPSC reversal potential (red trace; the EPSC on the red trace is scaled to the EPSC on the black trace). The feed-forward IPSC (green trace) was isolated by subtracting the red trace from the black trace. Note the larger EPSC on FS as compared to RS neurons.

(D) The amplitude of the EPSC recorded in the RS neuron is plotted against the amplitude of the simultaneously recorded EPSC in FS neurons for six experiments. Note the deviation of the experimental data points from the unity line. Inset, ratio between responses in FS and RS neurons. Red column, EPSCs; green column IPSCs. Summary graphs show mean ± SEM.

probabilities in FS units. Second, despite a reduction in spike probabilities, spike jitter should remain constant in FS units. We found this to be clearly the case. We recorded single RS and FS units in layer 4, identified by extracellular spike waveform (Bruno and Simons, 2002; Swadlow, 1989) (Figure 7C). FS units had broader receptive fields, consistent with previous reports (Bruno and Simons, 2002). By the fifth stimulus in a 10 Hz PW deflection train, spiking probabilities of FS units adapted to less than 15% of the initial probabilities. However, in striking contrast to RS units, the spike jitter did not significantly increase during the stimulus train (first stimulus, 4.07 ± 0.78; fifth stimulus, 4.55 ± 0.71; n = 34; $p > 0.05$) (Figure 7D). These results are in good agreement with the in vitro data reported above and strongly suggest that the temporal precision of cortical responses to whisker stimuli is dynamically regulated by a thalamocortical feed-forward inhibitory circuit.

A Simple Disynaptic Model for Thalamocortical Feed-Forward Inhibition

To test whether the cellular and synaptic properties determined above are sufficient to account for the dynamics of thalamocortical feed-forward inhibition, we devised a simple model of the circuit (Figure 8). The model includes an RS neuron and a pool of FS neurons

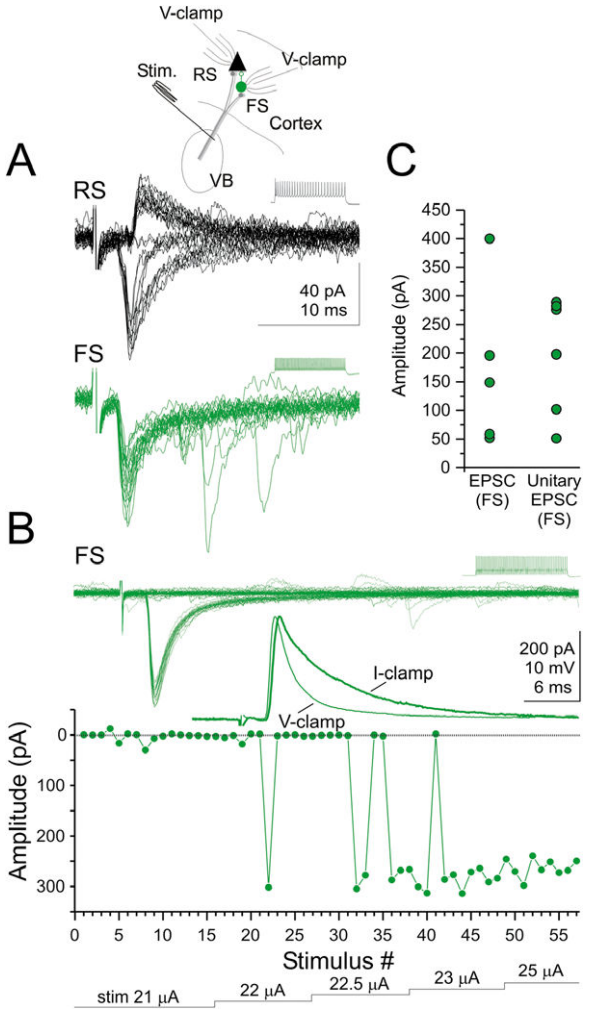

Figure 6. Very Few Thalamic Inputs Are Sufficient to Trigger Feed-Forward Inhibition

(A) Simultaneous voltage clamp recording from a RS (black traces, 27 superimposed sweeps) and a FS (green traces) neuron while stimulating the thalamus at threshold for eliciting feed-forward inhibition in the RS neuron. Note that in the RS neurons illustrated here direct thalamic EPSCs and feed-forward IPSCs occur or fail independently giving rise to four possible outcomes: EPSC-IPSC sequences, EPSCs only, IPSCs only, failures only.

(B) Voltage clamp recording ($V_{holding}$, −60 mV) from a FS neuron during minimal stimulation of the thalamus (58 superimposed sweeps). Note the relatively large amplitude of the unitary EPSC. Inset, average of successes recorded in current or voltage clamp. The amplitude of the unitary EPSP is 15 mV (Vm, −83 mV). Scatter plot, successes and failures of the unitary EPSCs plotted against stimulus intensity.

(C) Scatter plot comparing the amplitude of thalamic EPSCs recorded in FS neurons while stimulating the thalamus at threshold for triggering feed-forward inhibition in RS neurons (EPSC [FS], left column; n = 5) and the amplitudes of unitary EPSCs (right column; n = 6; same data set as in Figure 5B) evoked through minimal stimulation of the thalamus. Note the similarity of the two distributions.

and three types of synapse: from VB to FS, from FS to RS, and from VB to RS neurons. Model parameters were measured and fitted independently for each cell type and for each synapse type. All three synapse types exhibit depression to account for the experimental data (Figure 8A). We modeled synaptic depression as a decrease in resource (such as vesicles) available after each spike followed by recovery with an exponential time constant (Abbott et al., 1997; Tsodyks and Markram, 1997).

Because of the depression of the synapse from VB to FS neurons, after each stimulus, progressively fewer FS neurons reach threshold (Figure 8B). By the fifth stimulus, the fraction of FS neurons that reached threshold for action potential generation was down to about 20%. The reduced number of FS neurons spiking, combined with depression at synapses from FS to RS (Figure 8B), causes a pronounced decrease in feed-forward inhibition onto RS neurons (Figure 8C). Just as seen in the experimental observations (*dots*), the model (*traces*) predicts that by the end of the stimulus train feed-forward inhibition has decreased by about 90%. The effect of this decrease on the responses of the RS neuron is to substantially broaden the IW (Figure 8D). The components of this simple model are not only sufficient to explain the decrease in feed-forward inhibition (Figure 8C), but also necessary. Depression at the inhibitory synapse, on its own, is insufficient (Figure 8A, middle). The decrease in number of FS neurons that reach threshold, caused by the depression of the synapse onto FS neurons, is also insufficient on its own, especially to account for the pronounced reduction seen already at the second stimulus (Figure 8B). Only the combination of these effects achieves the observed decrease (Figure 8C).

This minimal model of the thalamocortical projection demonstrates how a disynaptic circuit accounts for a dynamic range of feed-forward inhibition that exceeds the dynamic range of each individual synapse in the circuit. Under the dynamic control of disynaptic IPSCs, RS neurons can act over a range of IWs, rapidly shifting from precise coincidence detectors to integrators.

Discussion

Keeping Time

Somatosensory stimuli trigger precisely time-locked responses in cortical neurons (Arabzadeh et al., 2005; Phillips et al., 1988). Such temporal accuracy is essential for sensory representation. We have found that thalamocortical feed-forward inhibition generated by a simple disynaptic circuit governs this temporal precision. We show that this circuit can narrow the integration IW to ~1 ms in barrel cortex neurons and thus may account for the temporal precision of these neurons to whisker stimulation (Arabzadeh et al., 2005; Petersen et al., 2001; Shimegi et al., 1999). Moreover, we show that the temporal window within which cortical neurons integrate thalamic activity (IW) is not fixed but can increase over an order of magnitude depending on the strength of feed-forward inhibition. The detailed in vitro analysis of the circuit resulted in testable predictions about the dynamics of RS and FS units during repetitive whisker stimulation in vivo. These predictions were verified by in vivo measurements of whisker-evoked spikes, strongly suggesting that feed-forward inhibitory circuits control temporal integration of somatosensory stimuli in vivo. Future manipulation of GABAergic transmission in vivo will allow more direct quantification of the contribution of inhibitory synapses

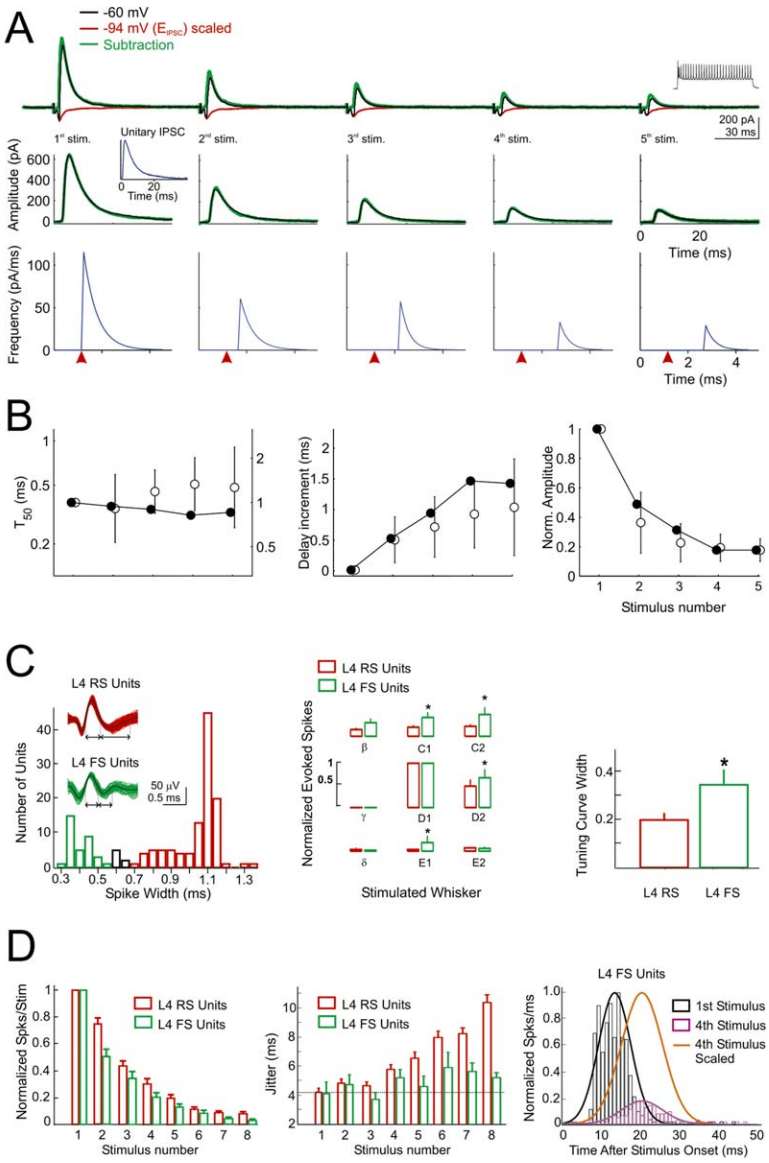

Figure 7. Temporal Precision Is Preserved in FS Neurons during Repetitive Stimulation

(A) Top row, response to 10 Hz thalamic stimulation in vitro of a layer 4 RS neuron voltage clamped at −60 mV (black trace) and at the IPSC reversal potential (red trace; the first EPSC on the red trace is scaled to the first EPSC on the black trace). The feed-forward IPSC (green trace) was isolated by subtracting the red trace from the black trace. Middle and lower rows, convolution of the "standard" unitary IPSC (inset, middle row) with the function $f(t) = (A/\tau) \times \exp(-t/\tau)$ (blue traces, lower row) provided a good fit (black traces, middle row) to the isolated feed-forward IPSC (green trace, middle row). Note in the lower panel, the progressively increasing delay of the onset of feed-forward inhibition after each stimulus. The delay in response to the first stimulus is marked by a red arrowhead.

(B) Left, time at which the integral over f(t) reaches 50% of its maximal value (T_{50}) plotted against stimulus number. The summary data (open symbols; n = 8) are normalized by the T_{50} of the first stimulus (right ordinate). Note that T_{50} changes little after each stimulus, despite the increase in delay (middle) and the decrease in amplitude (right) of feed-forward inhibition. Summary graphs show mean ± standard deviation.

(C) Identification of RS and FS units by total spike width (width of initial positive spike plus after hyperpolarization) in vivo. Left, histogram of total spike width across the population showing RS (red) and FS (green) units. Insets show examples of RS and FS unit waveforms. Center, mean whisker tuning curve for recording sites in D1 barrel. FS units had significantly broader tuning curves than RS units (asterisks, significant difference between FS and RS responses; $p < 0.05$; paired t test). Right, tuning curve width (mean ratio of adjacent surround whisker response to PW response) for all RS (n = 105) and FS (n = 34) units. Summary graphs show mean ± SEM.

(D) Response of RS and FS units to 10Hz whisker deflection. Left, spiking probability decreased for RS (n = 105) and FS (n = 34) units during the train. Both RS and FS units showed rapid adaptation (RS, AI = 0.19 ± 0.03; FS, AI = 0.13 ± 0.02, $p > 0.05$, t test). Middle, FS units did not show increased spike jitter during trains. Right, population PSTHS for first and fourth stimuli in train for all FS units. Note constant spike jitter despite adaptation and increased delay. Summary graphs show mean ± SEM.

to the encoding and behavioral discrimination of temporal stimulus features.

Feed-forward inhibitory circuits are ubiquitous in the brain (Shepherd, 1998) and have been shown to control neuronal excitability in time (Berger and Luscher, 2003; Blitz and Regehr, 2005; Brunel et al., 2004; Mittmann et al., 2005; Pouille and Scanziani, 2001; Wehr and Zador, 2003) and space (Laaris et al., 2000; Lavallee and Deschenes, 2004; London et al., 1989; Mountcastle and Powell, 1959; Petersen et al., 2001). The presence of thalamocortical feed-forward inhibitory circuits in the somatosensory "barrel cortex" is well documented both anatomically (Keller and White, 1987; Staiger et al., 1996) and physiologically (Agmon and Connors, 1991; Agmon and O'Dowd, 1992; Gil and Amitai, 1996; Porter et al., 2001; Swadlow and Gusev, 2000; Wilent and Contreras, 2004; Zhu and Connors, 1999).

We show that the efficiency of feed-forward inhibition in reducing the IW of neurons in the barrel cortex results from the concurrent action of at least four factors: first, a powerful thalamic synapse onto GABAergic fast spiking (FS) interneurons, such that the activity of only one or a few inputs is sufficient to trigger a spike; second, a fast "monosynaptic" delay (between the onset of the thalamic EPSC and the onset of the feed-forward IPSC) comprising 0.6 ms for thalamic EPSPs to reach spike threshold in FS neurons and additional 0.6 ms for the spike in FS neurons to propagate and release GABA on RS neurons; third, a high probability of connection between FS and RS neurons; and fourth, a large unitary IPSC conductance in RS neurons.

A caveat to the present findings is that our measure of the IW in RS neurons is based on the interaction between thalamically evoked EPSP-IPSP sequences and artificial

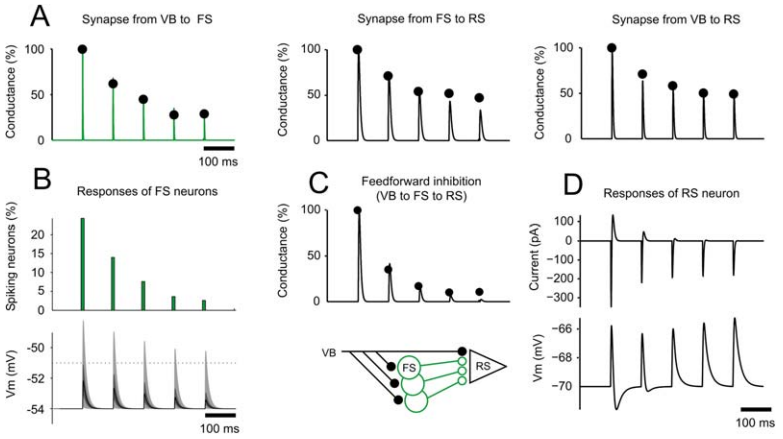

Figure 8. A Simple Disynaptic Model for Thalamocortical Feed-Forward Inhibition

(A) Conductance time course for the three synapses involved in the thalamocortical circuit (continuous traces) and experimental data (filled symbols; from Figures 3 and 4) plotted against time.

(B) Top, spiking probability of FS neurons. Bottom, distribution of membrane potentials in a simulated population of 100 FS neurons plotted against time. Light gray, all neurons; dark gray, half of the neurons (from the 25th to the 75th percentile); black trace, median (50th percentile). The dotted line indicates firing threshold.

(C) Top, time course of inhibitory conductances in RS neurons (feed-forward inhibition resulting from the spiking of the population of FS neurons excited by the thalamic input). Bottom, schematic illustration of the modeled circuit.

(D) Current (top) and voltage (bottom) time course in model RS neurons in response to 10 Hz thalamic activity. Note the progressive broadening of the half width of the postsynaptic potential.

EPSPs imposed with a somatic recording pipette. Thalamic afferents, however, impinge on the dendrites of RS neurons (Keller, 1995), whereas FS neurons preferentially (although not exclusively) project on the somatic/perisomatic compartment (Kawaguchi and Kubota, 1997; Markram et al., 2004; Somogyi et al., 1998). The spatial separation between excitatory and inhibitory inputs is likely to result in less shunting of thalamic EPSPs by feed-forward inhibitory conductances as compared to what observed on artificial EPSPs, suggesting that the duration of the IW in RS neurons may have been underestimated. This potential underestimation must be small, however, because the reduction of the amplitude of the artificial EPSP attributed to the shunt was only 15%.

Our recordings indicate that thalamic EPSCs in FS neurons are three times larger than in RS neurons, and this holds true for both unitary (Beierlein and Connors, 2002) and compound EPSCs. Hence, the stronger thalamic excitation of inhibitory FS as compared to excitatory RS cortical neurons is not merely due to an increased connectivity of thalamic inputs onto FS neurons. We propose that the large thalamic EPSC recorded in FS neurons may account, at least in part, for the high responsiveness of FS neurons to whisker stimulation (Bruno and Simons, 2002; Swadlow, 1989) and to spontaneous, single-thalamic spikes (Swadlow and Gusev, 2000) observed in vivo. Several not mutually exclusive possibilities could account for the difference in EPSC amplitude between FS and RS neurons, including a larger number of release sites per unitary input, a larger probability of release, a larger quantal amplitude, or a reduced membrane filtering of the postsynaptic EPSC. Elucidating the exact mechanism underlying this difference is the goal of future studies. The stronger depression of thalamic EPSCs onto FS neurons suggests that differences in release probability may account for at least part of the bias.

The faster decay kinetics of thalamic EPSCs on FS as compared to RS neurons is consistent with the kinetic differences observed for AMPA receptors obtained from these two types of neuron (Jonas et al., 1994) and, hence, is unlikely to be uniquely attributed to a difference in the membrane filtering of the signal. A large and fast EPSC is likely to significantly contribute to the temporally precise triggering of spikes in FS neurons (Fricker and Miles, 2000; Geiger et al., 1997; Jonas et al., 2004) and lead to the time-locked feed-forward IPSC.

Modulating the Integration Window

The dynamic range of the amplitude of thalamocortical feed-forward inhibition exceeds that of each individual synapse in the circuit and is responsible for the shift in the IW of RS neurons during repetitive thalamic stimulation. In principle, several properties of the circuit could contribute to the dynamic range, including the fraction of GABAergic interneurons recruited after each stimulus, the degree of synchrony of the recruited interneurons, the amount of GABA released on principal neurons, and their sensitivity to GABA. We show that spiking of FS neurons (in contrast to RS neurons) remains tightly time locked to each stimulus during the train, both in vivo and in vitro, suggesting that changes in synchrony do not contribute to the dynamics of feed-forward inhibition. The amplitude of the unitary IPSC decreased during repetitive presynaptic activity, but the magnitude of this depression is not sufficient to account for the full reduction in feed-forward inhibition. Rather, our data demonstrate that the broad dynamic range principally reflects the change in the fraction of GABAergic interneurons that are recruited by each thalamic stimulus. Our model shows that this change in fraction of recruited FS neurons can be well accounted for by the short-term dynamics of the thalamic input onto FS neurons. Although an activity-dependent reduction in the excitability of FS neurons could, in theory, also account for the observed reduction in the fraction of recruited FS neurons, two lines of evidence argue against this possibility. First, fast-spiking neurons show little spike adaptation to constant current injections and are, hence,

expected to adapt even less to brief phasic excitation separated by 100 ms. Second, the probability of spiking of FS neurons in response to a given whisker stimulus in a train is identical regardless of the success of the previous stimulus in the train to trigger a spike (data not shown).

The depression of thalamic EPSCs onto FS neurons is significantly larger than on RS neurons. This difference could be due to a postsynaptic property, namely a difference in the amount of and recovery from desensitization of AMPA receptors on the two types of neurons or to a presynaptic property, like the dynamic of transmitter release. We favor the second possibility because desensitization of AMPA receptors expressed in FS neurons recovers faster than in RS neurons (Jonas et al., 1994). Our physiological demonstration that a single thalamic fiber can impinge on both FS and RS neurons is consistent with anatomical evidence (see Figure 6F in Staiger et al., [1996]) and indicates that release properties from the thalamus are target cell specific.

Acute slices and anesthetized animals have low spontaneous activity compared to behaving animals. Thus, we were able to measure feed-forward inhibition at synapses that have "fully" recovered from previous activity, thus promoting strong feed-forward inhibition and narrow IWs. Increasing stimulus frequency to natural whisking frequency revealed the decrease in feed-forward inhibition and broadening of IWs. Thus, our experiments allowed us to explore the full dynamic range of thalamocortical feed-forward inhibition. In contrast, ongoing spontaneous thalamic activity in awake animals may depress thalamic inputs onto FS neurons even before the beginning of a whisking event (Castro-Alamancos, 2004), thereby reducing the dynamic range of feed-forward inhibition. However, in awake, behaving animals, neuromodulators and network activity may depolarize GABAergic interneurons such that even "depressed" thalamic inputs may be able to bring them to threshold for spike generation (Swadlow and Gusev, 2000), which would reduce the dynamic range of feed-forward inhibition but maintain narrow IWs. Hence, the actual magnitude of thalamocortical feed-forward inhibition, its dynamic range, and the resulting width of the IW in layer 4 neurons is likely to be strongly dependent on the behavioral state of the animal. The data presented here therefore illustrate the potential strength and dynamic range of thalamocortical feed-forward inhibition and demonstrate that this circuit can powerfully control and modulate temporal integration during the initial steps of somatosensory processing.

Experimental Procedures

All experiments were carried out in accordance with the guidelines set forth by the University of California.

Slices

Thalamocortical slices (400 μm) were prepared from 14–25 day old ICR White or C57BL/6 mice (Agmon and Connors, 1991; Porter et al., 2001) incubated for 40 min in an interface chamber at 35ºC with an artificial cerebrospinal fluid equilibrated with 95% O_2 and 5% CO_2, containing (in mM): 119 NaCl, 2.5 KCl, 1.3 $NaHPO_4$, 1.3 $MgCl_2$, 2.5 $CaCl_2$, 26 $NaHCO_3$, 20 glucose, and subsequently kept in the same chamber at room temperature for 0–6 hr until being transferred in a submerged chamber at 30ºC–33ºC for electrophysiological recordings.

In Vitro Thalamic Stimulation

Thalamic nuclei and barrels in the somatosensory cortex were first visualized with a low magnification objective with bright-field illumination and connectivity between the thalamus and the cortex assessed with a field-recording electrode (a patch pipette filled with 2 M NaCl) placed in the layer 4 of the barrel cortex while electrically stimulating thalamic afferents (stimulus duration, 100 μs; stimulus amplitude, 5–100 μA) with a monopolar steel electrode placed in the ventrobasal nucleus (VB) close to the border with the nucleus reticularis thalami, near the fimbria. We considered field responses of above 100 μV amplitude as acceptable evidence for a reliable connection. To ensure that the observed responses resulted from orthodromic stimulation of thalamocortical axons rather than antidromic stimulation of cortico-thalamic axons, we routinely determined three electrophysiological parameters of the response, namely latency, paired pulse ratio, and supernormality (Beierlein and Connors, 2002). We only considered experiments in which EPSPs recorded in layer 4 occurred at short latencies (<3.5 ms), showed paired pulse depression, and displayed no supernormality (i.e., decrease in latency of the second EPSP elicited 100 ms or less after the first).

In Vitro Recordings

Whole-cell recordings of visually identified neurons (infrared DIC videomicroscopy and water immersion objective [40×]) in layer 4 were obtained with patch pipettes (2–4 MΩ) containing (in mM): 150 K gluconate, 5 HEPES, 1.1 EGTA, 0.5–1 $MgCl_2$, 10 phosphocreatine, biocytin (0.1%–0.5%), and the pH adjusted to 7.2 with gluconic acid.

The firing pattern of the recorded neurons was determined immediately after rupturing the membrane by injecting 800 ms current pulses of incremental amplitude (50–600 pA) in the current-clamp mode. Regular spiking (RS) neurons were identified by their rapid adaptation of the instantaneous firing frequency in response to a square pulse of current (from a peak frequency of 161 ± 14 Hz [first two spikes] to a frequency of 29 ± 2 Hz [averaged over 100 ms, 400 ms after the beginning of the pulse]; 300–600 pA current injection; steady state to peak frequency ratio, 0.2 ± 0.02), a relatively long membrane time constant (16.6 ± 1 ms), a high input resistance in response to a 50 pA negative current pulse (232 ± 16 MΩ), and a relatively depolarized spike threshold (−49 ± 1 mV). Fast-spiking neurons were identified by a much less pronounced adaptation of the firing frequency (from a peak frequency of 106 ± 15 Hz [first two spikes] to a frequency of 92 ± 11 Hz [averaged over 100 ms, 400 ms after the beginning of the pulse]; 400–600 pA; steady state to peak frequency ratio, 1.1 ± 0.27), a faster membrane time constant (9.7 ± 1 ms), and a lower input resistance (81 ± 8 MΩ; spike threshold, −51 ± 1 mV; all values above were measured from a set of nine simultaneously recorded, FS/RS pairs) (Feldmeyer et al., 1999; Gibson et al., 1999; Kawaguchi and Kubota, 1997; McCormick et al., 1985). Low threshold spiking interneurons (Beierlein et al., 2003) were not included in the study.

In Vitro Data Acquisition and Analysis

Data were recorded with Multiclamp 700A or Axopatch 200B amplifiers, digitized at 5–10 kHz, and analyzed offline. Voltage measurements were corrected for the experimentally determined junction potential of 12 mV. Average values are expressed as mean ± SEM. The Student's t test was used for statistical comparisons. Electrophysiological traces illustrated in the figures represent the average averages about 10 to 40 individual sweeps, unless stated otherwise. To deconvolve the unitary IPSC from the feed-forward IPSC, we modeled the firing of FS neurons as occurring in a sharp onset followed by an exponential decay. This function is $f(t) = (A/\tau) \times \exp(-t/\tau)$, with parameters A and τ. We obtained these parameters by minimizing the square difference between the measured feed-forward IPSC and the convolution of f(t) with the unitary IPSC.

Dynamic Clamp

Dynamic clamp was used to simulate excitatory synaptic conductances, $g_{syn}(t)$, as follows: $I_{inj}(t) = g_{syn}(t) \times (Vm(t) - V_{rev})$, in which

$I_{inj}(t)$ is the current injected in the recorded neuron, Vm(t) is the membrane potential of the neuron, and V_{rev} is the reversal potential of the synaptic conductance to be simulated and was set at 0 mV. The time course of $g_{syn}(t)$ was given by the sum of two exponentials, τ_{rise} and τ_{decay}, of 0.15 and 1 ms, respectively. The amplitude ranged between 2 and 3 nS. The operation was performed with an analog circuit (5 MHz bandwidth) connected to the amplifier. Input and output signals were filtered at 5 kHz as described previously (Pouille and Scanziani, 2001). In three experiments, a standard current clamp configuration was used instead ($I_{inj}[t]$ independent of Vm) in which the time course of the I_{inj} was the same as g_{syn}, and the peak value of $I_{inj}(t)$ was either 100 or 200 pA.

In Vivo Recordings and Analysis

Long-Evans rats (P30–45) were anesthetized with urethane (Sigma, 1.5g/kg, i.p.) and prepared for acute recording as described previously (Celikel et al., 2004). Recordings were obtained with glass-insulated carbon fiber electrodes (0.5–1 MΩ at 1 kHz), or tungsten microelectrodes (2–4 MΩ at 1 kHz). Signals were preamplified (1,000×), band-pass filtered (0.5-10 kHz), further amplified (5×), and digitized at 32 kHz with custom Igor routines (Wavemetrics). Spike sorting was performed offline with a published algorithm (Fee et al., 1996) implemented in Matlab (Mathworks) by S. Mehta and D. Kleinfeld. Whiskers were deflected with calibrated, computer-controlled piezoelectric actuators 9 mm from the face. Initial mapping was performed to locate the barrel column of interest and layer 4 identified by depth and response latency (Celikel et al., 2004). Whisker deflections (250 μm ramp-and-hold deflection, 50 or 100 ms duration, rise/fall time 4 ms) were delivered at 0.5 Hz or in 10 Hz trains. 100 trials were collected at each recording site. Anesthesia was maintained by additional urethane (10% of original dose, i.p.) at a level that suppressed corneal and limb withdrawal reflexes and maintained breathing rate at <2 Hz. Columnar position and laminar location of all cortical recording sites were confirmed by lesion recovery (5 μA, 10 s) in cytochrome-oxidase-stained sections (Fox, 1992). Data analysis: spike counts and spike jitter were calculated for onset responses (spikes within 50 ms of deflection onset); spike jitter was defined as the standard deviation of the Gaussian fits of the onset PSTHs.

Model

This simple model of thalamocortical excitation and feed-forward inhibition includes three synapses (VB-FS, FS-RS, and VB-RS) each subject to synaptic depression (Figure 8). Each synapse type is described by only two parameters: a use factor u and the time constant of recovery τ_d. We obtained these parameters from responses to presynaptic trains at the following frequencies (in Hz): 2.5, 5, 10, 20, 50, and 100. Depression was pronounced at the synapse from VB to FS (u = 0.33, τ_D = 2.2 s) and less pronounced at the synapse from FS to RS (u = 0.26, τ_D = 4.1 s) and at the synapse from VB to RS (u = 0.60, τ_D = 0.2 s). FS neurons (n = 100) were described by an integrate-and-fire model with refractory period (R_{input} = 100 MΩ; τ_{mem}= 9.7 ms; V_{thresh} = −51 mV) and received a variable number of thalamic inputs such that the mean conductance of the thalamic EPSPs was 7.5 nS (with reversal potential E_{exc} = 0 mV) and varied by a factor of ten. We modeled the RS neuron as a single passive compartment (R_{input} = 200 MΩ; τ_{mem} = 16 ms) that receives an EPSC from VB (with reversal potential E_{exc} = 0 mV) and, 1 ms later, an IPSC from FS neurons (with reversal potential E_{inh} = −85 mV).

Acknowledgments

We thank the members of the Scanziani lab for comments on the manuscript and Stefan Baumann for help in the development of the model. This work was supported by the Swiss National Science Foundation (M.S. and M.C.) and National Institutes of Health grants MH71401 and MH70058 (M.S.) and the McKnight Foundation (D.E.F.).

Received: June 21, 2005
Revised: September 1, 2005
Accepted: September 22, 2005
Published: October 19, 2005

References

Abbott, L.F., Varela, J.A., Sen, K., and Nelson, S.B. (1997). Synaptic depression and cortical gain control. Science *275*, 220–224.

Agmon, A., and Connors, B.W. (1991). Thalamocortical responses of mouse somatosensory (barrel) cortex in vitro. Neuroscience *41*, 365–379.

Agmon, A., and O'Dowd, D.K. (1992). NMDA receptor-mediated currents are prominent in the thalamocortical synaptic response before maturation of inhibition. J. Neurophysiol. *68*, 345–349.

Arabzadeh, E., Zorzin, E., and Diamond, M.E. (2005). Neuronal encoding of texture in the whisker sensory pathway. PLoS Biol. *3*, e17.

Beierlein, M., and Connors, B.W. (2002). Short-term dynamics of thalamocortical and intracortical synapses onto layer 6 neurons in neocortex. J. Neurophysiol. *88*, 1924–1932.

Beierlein, M., Gibson, J.R., and Connors, B.W. (2003). Two dynamically distinct inhibitory networks in layer 4 of the neocortex. J. Neurophysiol. *90*, 2987–3000.

Berger, T., and Luscher, H.R. (2003). Timing and precision of spike initiation in layer V pyramidal cells of the rat somatosensory cortex. Cereb. Cortex *13*, 274–281.

Blitz, D.M., and Regehr, W.G. (2005). Timing and specificity of feed-forward inhibition within the LGN. Neuron *45*, 917–928.

Brecht, M., and Sakmann, B. (2002). Dynamic representation of whisker deflection by synaptic potentials in spiny stellate and pyramidal cells in the barrels and septa of layer 4 rat somatosensory cortex. J. Physiol. *543*, 49–70.

Brunel, N., Hakim, V., Isope, P., Nadal, J.P., and Barbour, B. (2004). Optimal information storage and the distribution of synaptic weights: perceptron versus Purkinje cell. Neuron *43*, 745–757.

Bruno, R.M., and Simons, D.J. (2002). Feedforward mechanisms of excitatory and inhibitory cortical receptive fields. J. Neurosci. *22*, 10966–10975.

Buracas, G.T., Zador, A.M., DeWeese, M.R., and Albright, T.D. (1998). Efficient discrimination of temporal patterns by motion-sensitive neurons in primate visual cortex. Neuron *20*, 959–969.

Castro-Alamancos, M.A. (2004). Absence of rapid sensory adaptation in neocortex during information processing states. Neuron *41*, 455–464.

Celikel, T., Szostak, V.A., and Feldman, D.E. (2004). Modulation of spike timing by sensory deprivation during induction of cortical map plasticity. Nat. Neurosci. *7*, 534–541.

Chung, S., Li, X., and Nelson, S.B. (2002). Short-term depression at thalamocortical synapses contributes to rapid adaptation of cortical sensory responses in vivo. Neuron *34*, 437–446.

Coombs, J.S., Eccles, J.C., and Fatt, P. (1955). The inhibitory suppression of reflex discharges from motoneurones. J. Physiol. *130*, 396–413.

DeWeese, M.R., Wehr, M., and Zador, A.M. (2003). Binary spiking in auditory cortex. J. Neurosci. *23*, 7940–7949.

Fee, M.S., Mitra, P.P., and Kleinfeld, D. (1996). Automatic sorting of multiple unit neuronal signals in the presence of anisotropic and non-Gaussian variability. J. Neurosci. Methods *69*, 175–188.

Feldmeyer, D., Egger, V., Lubke, J., and Sakmann, B. (1999). Reliable synaptic connections between pairs of excitatory layer 4 neurones within a single 'barrel' of developing rat somatosensory cortex. J. Physiol. *521*, 169–190.

Fox, K. (1992). A critical period for experience-dependent synaptic plasticity in rat barrel cortex. J. Neurosci. *12*, 1826–1838.

Fricker, D., and Miles, R. (2000). EPSP amplification and the precision of spike timing in hippocampal neurons. Neuron *28*, 559–569.

Geiger, J.R., Lubke, J., Roth, A., Frotscher, M., and Jonas, P. (1997). Submillisecond AMPA receptor-mediated signaling at a principal neuron-interneuron synapse. Neuron *18*, 1009–1023.

Gibson, J.R., Beierlein, M., and Connors, B.W. (1999). Two networks of electrically coupled inhibitory neurons in neocortex. Nature *402*, 75–79.

Gil, Z., and Amitai, Y. (1996). Properties of convergent thalamocortical and intracortical synaptic potentials in single neurons of neocortex. J. Neurosci. *16*, 6567–6578.

Gil, Z., Connors, B.W., and Amitai, Y. (1999). Efficacy of thalamocortical and intracortical synaptic connections: quanta, innervation, and reliability. Neuron *23*, 385–397.

Jonas, P., Racca, C., Sakmann, B., Seeburg, P.H., and Monyer, H. (1994). Differences in Ca^{2+} permeability of AMPA-type glutamate receptor channels in neocortical neurons caused by differential GluR-B subunit expression. Neuron *12*, 1281–1289.

Jonas, P., Bischofberger, J., Fricker, D., and Miles, R. (2004). Interneuron Diversity series: fast in, fast out—temporal and spatial signal processing in hippocampal interneurons. Trends Neurosci. *27*, 30–40.

Kawaguchi, Y., and Kubota, Y. (1997). GABAergic cell subtypes and their synaptic connections in rat frontal cortex. Cereb. Cortex *7*, 476–486.

Keller, A. (1995). Synaptic Organization of the Barrel Cortex, *Volume 11* (New York, NY: Plenum Press).

Keller, A., and White, E.L. (1987). Synaptic organization of GABAergic neurons in the mouse SmI cortex. J. Comp. Neurol. *262*, 1–12.

Khatri, V., Hartings, J.A., and Simons, D.J. (2004). Adaptation in thalamic barreloid and cortical barrel neurons to periodic whisker deflections varying in frequency and velocity. J. Neurophysiol. *92*, 3244–3254.

Koch, C., Rapp, M., and Segev, I. (1996). A brief history of time (constants). Cereb. Cortex *6*, 93–101.

Konig, P., Engel, A.K., and Singer, W. (1996). Integrator or coincidence detector? The role of the cortical neuron revisited. Trends Neurosci. *19*, 130–137.

Laaris, N., Carlson, G.C., and Keller, A. (2000). Thalamic-evoked synaptic interactions in barrel cortex revealed by optical imaging. J. Neurosci. *20*, 1529–1537.

Lavallee, P., and Deschenes, M. (2004). Dendroarchitecture and lateral inhibition in thalamic barreloids. J. Neurosci. *24*, 6098–6105.

Lloyd, D.P.C. (1946). Facilitation and inhibition of spinal motoneurons. J. Neurophysiol. *9*, 421–438.

London, J.A., Cohen, L.B., and Wu, J.Y. (1989). Optical recordings of the cortical response to whisker stimulation before and after the addition of an epileptogenic agent. J. Neurosci. *9*, 2182–2190.

Markram, H., Toledo-Rodriguez, M., Wang, Y., Gupta, A., Silberberg, G., and Wu, C. (2004). Interneurons of the neocortical inhibitory system. Nat. Rev. Neurosci. *5*, 793–807.

McCormick, D.A., Connors, B.W., Lighthall, J.W., and Prince, D.A. (1985). Comparative electrophysiology of pyramidal and sparsely spiny stellate neurons of the neocortex. J. Neurophysiol. *54*, 782–806.

Mittmann, W., Koch, U., and Hausser, M. (2005). Feed-forward inhibition shapes the spike output of cerebellar Purkinje cells. J. Physiol. *563*, 369–378.

Mountcastle, V.B. (1968). Medical Physiology, *Volume 2*, Twelfth Edition (St. Louis, MO: Mosby).

Mountcastle, V.B., and Powell, T.P. (1959). Neural mechanisms subserving cutaneous sensibility, with special reference to the role of afferent inhibition in sensory perception and discrimination. Bull. Johns Hopkins Hosp. *105*, 201–232.

Petersen, R.S., Panzeri, S., and Diamond, M.E. (2001). Population coding of stimulus location in rat somatosensory cortex. Neuron *32*, 503–514.

Phillips, J.R., Johnson, K.O., and Hsiao, S.S. (1988). Spatial pattern representation and transformation in monkey somatosensory cortex. Proc. Natl. Acad. Sci. USA *85*, 1317–1321.

Porter, J.T., Johnson, C.K., and Agmon, A. (2001). Diverse types of interneurons generate thalamus-evoked feedforward inhibition in the mouse barrel cortex. J. Neurosci. *21*, 2699–2710.

Pouille, F., and Scanziani, M. (2001). Enforcement of temporal fidelity in pyramidal cells by somatic feed-forward inhibition. Science *293*, 1159–1163.

Reinagel, P., and Reid, R.C. (2000). Temporal coding of visual information in the thalamus. J. Neurosci. *20*, 5392–5400.

Shepherd, G.M. (1998). The Synaptic Organization of the Brain, Fourth Edition (New York, NY: Oxford University Press).

Shimegi, S., Ichikawa, T., Akasaki, T., and Sato, H. (1999). Temporal characteristics of response integration evoked by multiple whisker stimulations in the barrel cortex of rats. J. Neurosci. *19*, 10164–10175.

Somogyi, P., Tamas, G., Lujan, R., and Buhl, E.H. (1998). Salient features of synaptic organisation in the cerebral cortex. Brain Res. Brain Res. Rev. *26*, 113–135.

Staiger, J.F., Zilles, K., and Freund, T.F. (1996). Distribution of GABAergic elements postsynaptic to ventroposteromedial thalamic projections in layer IV of rat barrel cortex. Eur. J. Neurosci. *8*, 2273–2285.

Stratford, K.J., Tarczy-Hornoch, K., Martin, K.A., Bannister, N.J., and Jack, J.J. (1996). Excitatory synaptic inputs to spiny stellate cells in cat visual cortex. Nature *382*, 258–261.

Swadlow, H.A. (1989). Efferent neurons and suspected interneurons in S-1 vibrissa cortex of the awake rabbit: receptive fields and axonal properties. J. Neurophysiol. *62*, 288–308.

Swadlow, H.A., and Gusev, A.G. (2000). The influence of single VB thalamocortical impulses on barrel columns of rabbit somatosensory cortex. J. Neurophysiol. *83*, 2802–2813.

Tarczy-Hornoch, K., Martin, K.A., Jack, J.J., and Stratford, K.J. (1998). Synaptic interactions between smooth and spiny neurones in layer 4 of cat visual cortex in vitro. J. Physiol. *508*, 351–363.

Tsodyks, M.V., and Markram, H. (1997). The neural code between neocortical pyramidal neurons depends on neurotransmitter release probability. Proc. Natl. Acad. Sci. USA *94*, 719–723.

Wehr, M., and Zador, A.M. (2003). Balanced inhibition underlies tuning and sharpens spike timing in auditory cortex. Nature *426*, 442–446.

Wilent, W.B., and Contreras, D. (2004). Synaptic responses to whisker deflections in rat barrel cortex as a function of cortical layer and stimulus intensity. J. Neurosci. *24*, 3985–3998.

Zhu, J.J., and Connors, B.W. (1999). Intrinsic firing patterns and whisker-evoked synaptic responses of neurons in the rat barrel cortex. J. Neurophysiol. *81*, 1171–1183.